Supporting Information

In vivo molecular photoacoustic tomography of melanomas targeted by bio-conjugated gold nanocages

CHULHONG KIM[1†], EUN CHUL CHO[1†], JINGYI CHEN[1], KWANG HYUN SONG[1], LESLIE AU[1], CHRISTOPHER FAVAZZA[1], QIANG ZHANG[1], CLAIRE M. COBLEY[1], FENG GAO[2], YOUNAN XIA,[1]* AND LIHONG V. WANG[1]*

[1]Department of Biomedical Engineering, Washington University in St. Louis, St. Louis, Missouri 63130, USA

[2]Division of Biostatistics, Washington University School of Medicine, St. Louis, Missouri 63110, USA

[†] These two authors contributed equally to this work.

*Corresponding authors

Lihong V. Wang for photoacoustic tomography, lhwang@biomed.wustl.edu

Younan Xia for gold nanocages and bio-conjugation, xia@biomed.wustl.edu

Supporting Notes

Photoacoustic tomography (PAT)

In PAT, the subject is irradiated by a short-pulsed laser beam. Some of the light is absorbed by the target, partially converted into heat, and then further converted to a pressure increase via thermo-elastic expansion (referred to as the photoacoustic (PA) effect). This initial pressure rise is determined by the local optical energy deposition (the product of local optical absorption coefficient and local optical fluence) and other thermal and mechanical properties. The propagated acoustic waves in biological tissues are detected by ultrasonic transducers. By measuring acoustic pressures as a function of the arrival times, images are produced to represent optical absorption heterogeneities in tissues. Therefore, PAT provides strong optical absorption contrasts (PA excitation phase) with high ultrasonic spatial resolution (PA emission phase). Since ultrasonic scattering is 2-3 orders of magnitude less than optical scattering, PA imaging can overcome the limitations of existing pure optical imaging (i.e., shallow imaging depth, typically <1 mm, for high resolution or low spatial resolution beyond 1 mm) and pure ultrasonic imaging (i.e., weak contrast for early cancer detection and speckle artifacts). Using intrinsic contrasts such as hemoglobin or melanin, PA imaging plays important roles in cancer research by showing tumor angiogenesis and tumor hypoxia, dynamic functional brain imaging, and internal organ imaging, among others. Furthermore, taking advantages of exogenous contrast agents (organic dyes, nanoparticles, and reporter genes), this imaging modality has become increasingly important in molecular imaging and noninvasive sentinel lymph node mapping.

Supporting Figures

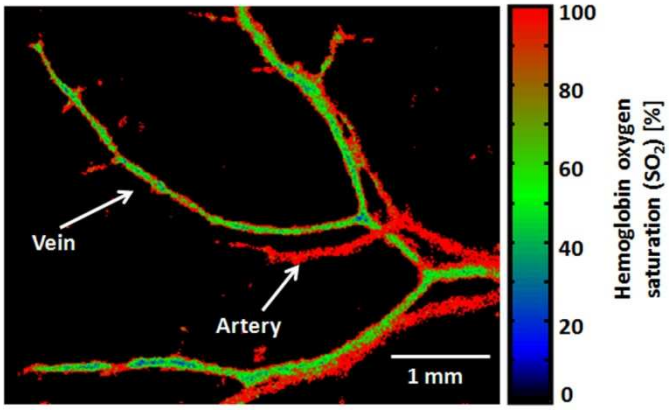

Figure S1. Noninvasive *in vivo* PA mapping of hemoglobin oxygen saturation (SO_2) in the skin of a normal mouse. The average SO_2 values in arteries and veins are 90 ± 6% and 65 ± 8 %, respectively.

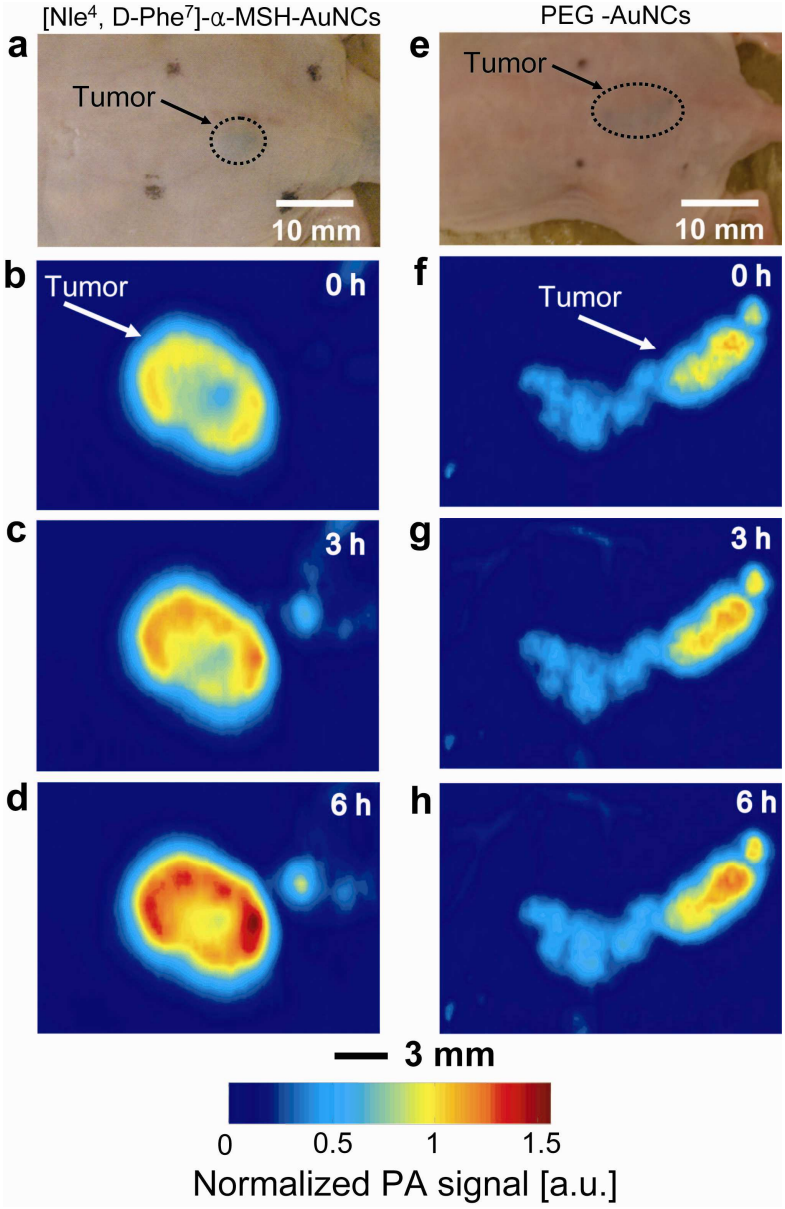

Figure S2. Noninvasive *in vivo* PA time-course coronal MAP images of B16 melanomas using [Nle^4,D-Phe^7]-α-MSH- and PEG-AuNCs. a and **e**, Photographs of nude mice transplanted with B16 melanomas before injection of (**a**) [Nle^4,D-Phe^7]-α-MSH- and (**e**) PEG-AuNCs. **b-d** and **f-h**, Time-course PA images of the B16 melanomas after intravenous injection with 100 μL of 10-nM (**b-d**) [Nle^4,D-Phe^7]-α-MSH- and (**f-h**) PEG-AuNCs through the tail vein. The melanoma images were obtained using the PA macroscope at 778 nm (ultrasonic frequency: 10 MHz).

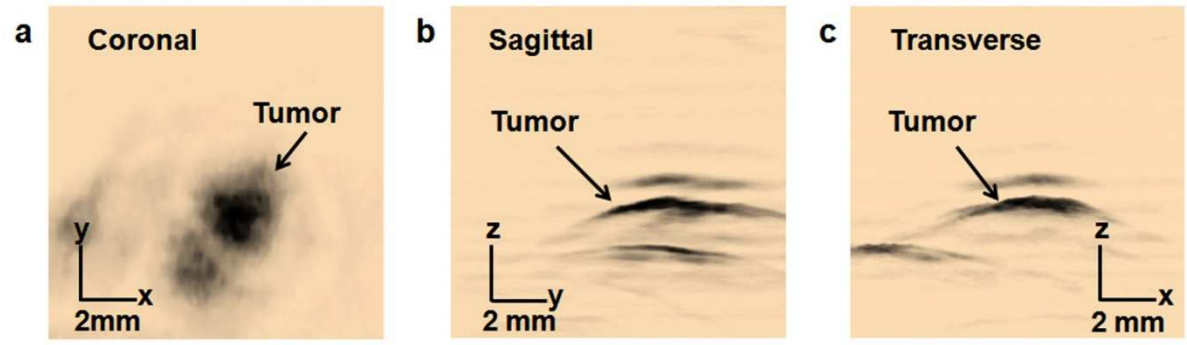

Figure S3. Noninvasive *in vivo* PA MAP images of a deeply positioned melanoma. The imaging depth was increased to 1.2 cm by adding chicken tissues onto the skin of the mouse, and a 5-MHz ultrasound transducer was used. Three types of MAP images are shown: **a**, Coronal; **b**, sagittal; and **c**, transverse.

Supporting Methods

Measuring the detection sensitivity of the PA imaging system

We used an optically scattering medium to prevent direct illumination of the sample by light, protecting the gold nanocages (AuNC) from deformation. Two Tygon® tubes were embedded at 1-mm depth from the surface of the optically scattering medium. One tube was then filled with aqueous suspensions of the AuNC at various concentrations, and the other was filled with water. When the solution was illuminated by the laser, the generated PA waves were detected by a single-element 10-MHz ultrasound transducer.

Measuring optical absorption cross-sections of AuNC

We obtained the extinction coefficients (μ_e) of the AuNC from their UV-vis-NIR spectra and the Beer-Lambert law (Fig. S4). The experimental setup and procedures were described in Ref. 26 of the manuscript. A light source of 778 nm was used. We acquired optical absorption coefficients of AuNC ($\mu_{a,AuNC}$) by using a calibration curve derived from the linear relationship between the PA signal and absorption coefficient (μ_a) of indocyanine green (ICG) solutions at various concentrations. In this case, we measured the PA signals from aqueous solutions of ICG at various concentrations, and then plotted the μ_a against the PA signal to derive the linear correlation (Fig. S5). We obtained μ_a of ICG from UV-vis-NIR spectrum at 778 nm. The linear dependence in Fig. S5 can be described using the following empirical equation:

$$\mu_a = 2.74 \times \text{PA signal} - 0.16 . \quad \text{(S1)}$$

After obtaining $\mu_{a,AuNC}$ from equation (S1) and PA signals measured at the concentrations shown in Fig. 1e, we calculated their absorption cross-sections using the following equation:

$$\mu_{a,AuNC} = N_{AuNC}\sigma_{a,AuNC} , \quad \text{(S2)}$$

where $\sigma_{a,AuNC}$ is the absorption cross-section (m^2), and N_{AuNC} is the concentration of the AuNC (number of particles per m^3). The measured extinction and absorption cross-sections of AuNC were 2.49×10^{-14} m^2 and 1.73×10^{-14} m^2, respectively. The ratio of absorption to extinction cross-sections is 0.7, which implies that the AuNCs are dominated by absorption.

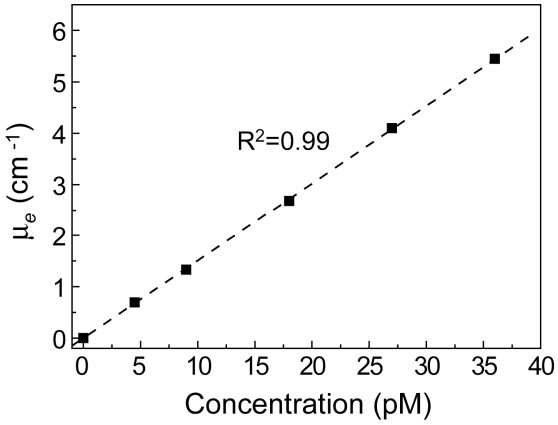

Supplementary Figure S4. A plot for the extinction coefficient (μ_e) versus concentration of AuNCs. According to the Beer-Lambert law, the extinction cross-section of AuNCs was 2.5×10^{-14} m^2.

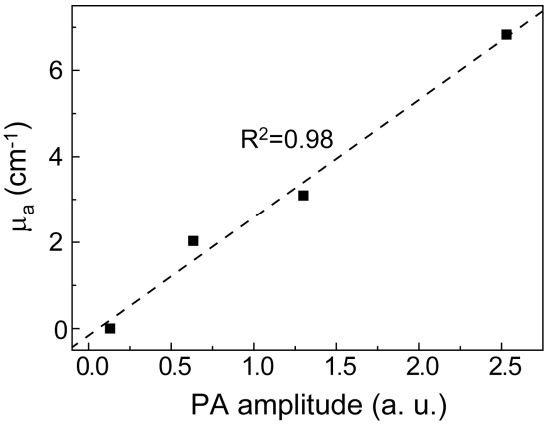

Supplementary Figure S5. A linear relationship between optical absorption coefficient (μ_a) and PA signal amplitude of ICG. We obtained μ_a from the UV-vis-NIR spectrum of ICG at 778 nm.

Mapping of oxygen saturation of hemoglobin (SO_2)

In PA measurements of SO_2, hemoglobin is considered a dominant optical absorption chromophore at each wavelength (λ_i). The two forms of hemoglobin, oxy- and deoxy-hemoglobins, have different molar extinction spectra (Fig. S6).

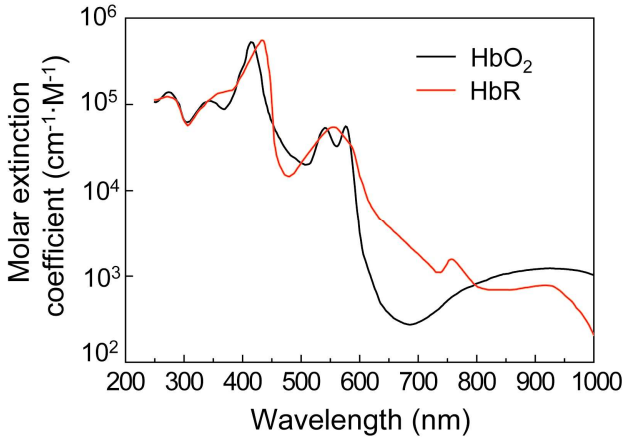

Figure S6. Spectra of two types of hemoglobin. Oxy-hemoglobin (HbO_2) and deoxy-hemoglobin (HbR).

Using a first order approximation, the blood absorption coefficient $\mu_a(\lambda_i)$ can be estimated as follows:

$$\mu_a(\lambda_1) = \varepsilon_{ox}(\lambda_1)C_{ox} + \varepsilon_{de}(\lambda_1)C_{de}, \quad \text{(S3)}$$

$$\mu_a(\lambda_2) = \varepsilon_{ox}(\lambda_2)C_{ox} + \varepsilon_{de}(\lambda_2)C_{de}, \quad \text{(S4)}$$

where μ_a (cm^{-1}) is the absorption coefficient; λ_1 and λ_2 are the two wavelengths; ε_{ox} and ε_{de} are the known molar extinction coefficients (cm^{-1} mM^{-1}) of the HbO_2 and HbR, respectively; C_{ox} and C_{de} are the concentrations (mM) of the two forms of hemoglobin. Using Eqs (S3) and (S4), the SO_2 can be calculated, $SO_2 = C_{ox}/(C_{ox} + C_{de})$. More than two optical wavelengths can be applied to improve accuracy.

Estimating the number of [Nle^4,D-Phe^7]-α-MSH-AuNCs accumulated in the melanoma based on the increase in PA signal

Assumptions

1) The AuNCs were evenly distributed in the melanoma.

2) A 38% PA signal increase was observed during *in-vivo* PA imaging. From the sensitivity test (Fig. 1e), 3 pM of AuNCs is necessary for a 38% increase in the PA signal. However, 4.5 pM was used in the estimation, because it was the lowest measured sensitivity value obtained from the current PA imaging system.

Calculation

1. The dimensions of one resolution voxel are 125 and 140 μm along the axial and transverse directions, respectively. Therefore, the volume is calculated to be $125 \times \pi \times 70^2$ μm^3 = 1.90×10^{-12} m^3 (1.90×10^{-9}L).
2. The moles of nanocages per voxel is (4.5×10^{-12} moles/L) × (1.90×10^{-9} L) = 8.55×10^{-21} moles. Therefore, the number of AuNCs per one voxel is calculated to be (8.55×10^{-21}) × (6.02×10^{23}) = 5.15×10^3/voxel.
3. The average volume of the tumor was 7.98×10^{-9} m^3 (based on the image analysis of 4 tumors used for target-sensitive AuNCs), hence the number of imaging voxels in this tumor is 4.20×10^3.
4. By multiplying the number of voxels by the number of AuNCs in one voxel, we can obtain the number of AuNCs in the tumor, (4.20×10^3) × (5.15×10^3/voxel) = 2.16×10^7. The average mass of the tumor was measured to be 27 mg so that the number can be normalized to be 8.00×10^8 per tumor mass (g).

The ICP results: 3.6×10^8 AuNCs per gram of tumor (the error was 55%, or the ratio of experimental to estimated AuNCs was 0.45)